Silica Adsorbent Design and Process Evaluation for Recovery of Homogeneous Catalysts by Reverse Flow Adsorption

T. Dekic Zivkovic and A. B. de Haan
Dept. of Chemical Engineering and Chemistry, Eindhoven University of Technology, Eindhoven, The Netherlands

DOI 10.1002/aic.11541
Published online July 21, 2008 in Wiley InterScience (www.interscience.wiley.com).

The goal of this work is to demonstrate the stability of reverse flow adsorption process for recovery of homogeneous catalysts and to study the influence of catalyst and adsorbent properties for optimizing the RFA process operation. Data used in simulations were obtained from our previous work. Two models are developed to describe the reversible adsorption. One which describes the adsorption of the metal containing species and second model that describes adsorption of the free ligand. It is shown that stable operation is reached, where leaching of metal is prevented. The RFA process can be applied for wide ranges of the catalyst's stability constants [10^0–10^{12} $(dm^3/mol)^2$] and it is specially applicable for the recovery of homogeneous catalysts that have a low metal concentration. Values of the adsorbent ($\beta_M = 0.8$, $\alpha = 1850$, $Pe_P = 376.4$, $d_p = 100$ μm and $\varepsilon_b = 0.5$) and the column characteristics ($Bo = 1.74 \times 10^4$ and $N = 6.6 \times 10^4$) that provide a sharp concentration profile inside the bed are determined. Simulation of the recovery of Rh catalyst in the BASF hydroformylation process required a total adsorption bed volume of 6% of reactor volume. © 2008 American Institute of Chemical Engineers *AIChE J*, 54: 2392–2403, 2008

Keywords: adsorption, reverse flow, homogeneous catalysts, modeling, design

Introduction

The reverse flow concept is mainly used in the field of reactor engineering, where Boreskov and Matros[1,2] were among the first researchers working on reverse flow reactors. Since then many scientists contributed to this field.[3–5] Besides its use in reactor design, the reverse flow concept was also used in electrokinetic chromatography[6] and nano- and ultra-filtration.[7,8]

Reverse flow adsorption (RFA) is a novel concept for the recovery of homogenous catalysts that combines separation by adsorption with reverse flow technology.[9] In RFA, the feed (reactants, homogeneous catalyst, and solvent) periodically changes its direction in the process. The homogeneous catalyst is separated from the reaction mixture by adsorption downstream from the reactor (Figure 1). In the subsequent desorption step the homogenous catalyst is recovered and recycled to the reactor. This approach should overcome drawbacks of present recovery methods, such as leaching and deactivation of the catalyst.[10] Leaching can be prevented by designing the RFA process in a way that all catalyst species are kept inside the beds. Adsorption process properties can be either at the reaction conditions or at the conditions more favorable for constant activity of the catalyst.

Since a homogeneous catalyst is found in different complex forms,[11] we propose to recover the catalyst using a two-step adsorption approach: separately adsorbing the metal containing species from the excess of ligand. The metal containing catalyst species are adsorbed from the reactor effluent in the first adsorption bed, whereas the remaining free ligand is

Correspondence concerning this article should be addressed to T. D. Zivkovic at t.djekic@tue.nl.

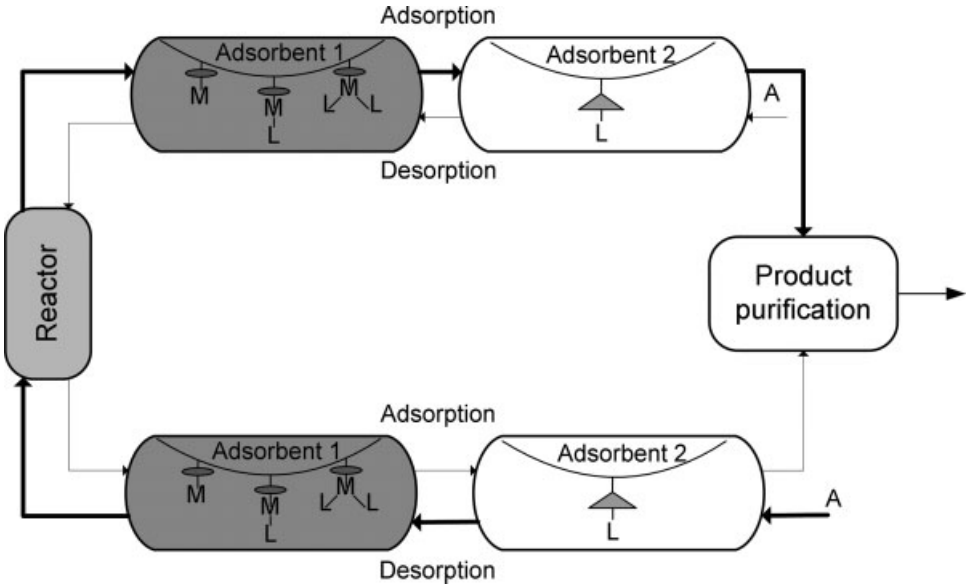

Figure 1. Reverse Flow Adsorption concept for the recovery of homogeneous catalysts.

adsorbed in the second adsorption bed. For this reason four adsorption beds are needed to adsorb homogenous catalysts by the two step approach (Figure 1). Dunnewijk, who also worked on the RFA concept,[12] also applied the two-step adsorption approach. Their focus was on separate adsorption of the free metal center and the free ligand by neglecting any interaction between them. Bidispersed polymer type and gel type adsorbents were selected to recover the free metal and the free ligand, but this material was prone to swelling and showed very slow mass transfer.[13] Additionally, selected adsorbents were mostly either very strong or rather weak for reversible adsorption of the homogeneous catalysts species.[14] Dunnewijk[12] also developed a model to simulate the RFA process which consisted of two adsorption columns and a CIST reactor. He showed stability of the RFA process with the data obtained from ion-exchange experiments excluding micropore diffusion. The drawbacks of polymeric adsorbents directed our research to functionalized silica adsorbents which have a mesoporous and rigid structure. In our previous work, we showed promising intermediate adsorbents,[15,16] with sufficiently high mass transfer coefficients [Djekić T, Tripkovic V, van der Ham AGJ, de Haan AB. Intraparticle diffusion coefficients of $CoCl_2$ in mesoporous functionalized silica adsorbents. *Adsorption*. (submitted)].

The objective of this work is to demonstrate stable operation of the RFA process with the data obtained from functionalized silica adsorbents [Djekić T, Tripkovic V, van der Ham AGJ, de Haan AB. Intraparticle diffusion coefficients of $CoCl_2$ in mesoporous functionalized silica adsorbents. *Adsorption*. (submitted)].[15,16] and to study the influence of adsorbent and process parameters to improve RFA operation. Design and study of the reactor is not included since extensive studies on the reverse flow reactors are already carried out, as mentioned previously.[1–5] This article proceeds with the mathematical models developed to describe reversible adsorption of the complex species. One model describes the reversible adsorption of the metal containing species and other model describes adsorption of the free ligand. The first model is more complex because it contains competitive adsorption of different complex forms which are via a chemical equilibrium interconnected in solution.[11] Therefore, stability of the process is initially shown by monitoring the total metal concentration (sum of all metal containing species) profile during continuous adsorption and desorption for 500 cycles. Furthermore, the influences of the adsorbent and process parameters are discussed as well as application for different catalyst characteristics such as concentration, stability constants, or ligand to metal ratio. These effects are studied with our first model that describes the adsorption of the metal containing species. Their optimized values are afterwards applied for the ligand bed. Finally, the application of the RFA is evaluated for the BASF hydroformylation process[17] with the evaluation of several adsorption bed designs to obtain maximal operation time.

Dynamic Models for the Reversible Adsorption of the Catalyst Species

To simulate the RFA process two models are developed: one for adsorption of the metal containing species, and the other for adsorption of the free ligand. Similarities and differences between those two models are listed in Table 1. Both models are written in their dimensionless forms and the nomenclature is given in the Symbol section.

In the previous work of Dunnewijk[12] it is shown that adsorption beds used in the RFA process should be preloaded with the adsorbing specie to allow broadening of the concentration front during its reversible adsorption and desorption. This effect is described in our simulations by setting proper initial conditions (see Section Model for adsorption of metal containing species). Stability of the process and optimization of the adsorbent/process parameters are shown by simulating reversible adsorption of the catalyst species in just one bed. A change of concentration in the bed is monitored over time and in axial direction.

Table 1. Similarities and Differences Between the Model for Adsorption of the Metal Containing Species and the Model for Adsorption of the Free Ligand

Model for Adsorption of Metal Containing Species	Model for Adsorption of Free Ligand
Similarity	
Dimensionless	
Negligible external mass transfer resistance	
Internal mass transfer described by linear driving force model	
Negligible radial concentration gradient	
Constant bed porosity (exclusion of channelling)	
Constant velocity across the cross-section	
Preloaded columns	
Same process parameters	
Difference	
Stability Constants-Equilibrium is Infinitely Fast	–
Competitive Langmuir Isotherm	Langmuir Isotherm for Single Component
Different adsorbent parameters	
Different bed parameters	

Model for adsorption of the metal containing species

Stability Constants. In this model it is assumed that the homogeneous catalyst is a complex compound consisting of one metal center and two ligands. Dissolved in a solvent a homogenous catalyst forms different species:

$$\mathrm{M} + 2\mathrm{L} \underset{\longleftarrow}{\overset{K_{S1}}{\longrightarrow}} \mathrm{ML} + \mathrm{L} \underset{\longleftarrow}{\overset{K_{S2}}{\longrightarrow}} \mathrm{ML_2}. \tag{1}$$

The ratio of different species at equilibrium is described by stability constants presented as

$$\kappa_{S1} = \frac{x_{\mathrm{ML}}(\chi,\tau)}{x_{\mathrm{M}}(\chi,\tau)\cdot x_{\mathrm{L}}(\chi,\tau)} \tag{2}$$

$$\kappa_{S2} = \frac{x_{\mathrm{ML_2}}(\chi,\tau)}{x_{\mathrm{ML}}(\chi,\tau)\cdot x_{\mathrm{L}}(\chi,\tau)}. \tag{3}$$

Competitive Adsorption Isotherm. In our previous work,[13] we have shown that all metal containing species (M, ML, and ML_2) are adsorbing on one active site of the adsorbent and their adsorption can be described with the competitive Langmuir isotherm

$$\Gamma_{\mathrm{M}}(z,t) = \frac{\beta_{\mathrm{M}}\cdot x_{\mathrm{M}}(\chi,\tau)}{1+\beta_{\mathrm{M}}\cdot x_{\mathrm{M}}(\chi,\tau)+\beta_{\mathrm{ML}}\cdot x_{\mathrm{ML}}(\chi,\tau)+\beta_{\mathrm{ML_2}}\cdot x_{\mathrm{ML_2}}(\chi,\tau)} \tag{4}$$

Equivalent equations can be written for ML and ML_2.The total amount of metal adsorbed is described as

$$\Gamma_{\mathrm{M_t}}(\chi,\tau) = \Gamma_{\mathrm{M}}(\chi,\tau) + \Gamma_{\mathrm{ML}}(\chi,\tau) + \Gamma_{\mathrm{ML_2}}(\chi,\tau) \tag{5}$$

Mass Balance for the Liquid Phase in Adsorption Bed. The dimensionless mass balance for the liquid phase is given for the total amounts of metal in the system, M_t

$$\mathrm{FD}\cdot\frac{1}{\varepsilon_t}\frac{\partial x_{\mathrm{M_t}}(\chi,\tau)}{\partial\chi} + \frac{\partial x_{\mathrm{M_t}}(\chi,\tau)}{\partial\tau} + \frac{1-\varepsilon_t}{\varepsilon_t}\alpha\frac{\partial\bar{\Gamma}_{\mathrm{M_t}}(\chi,\tau)}{\partial\tau} = \frac{1}{Bo}\frac{\partial^2 x_{\mathrm{M_t}}(\chi,\tau)}{\partial\chi^2} \tag{6}$$

$$x_{\mathrm{M_t}}(\chi,\tau) = x_{\mathrm{M}}(\chi,\tau) + x_{\mathrm{ML}}(\chi,\tau) + x_{\mathrm{ML_2}}(\chi,\tau), \tag{7}$$

and ligand L_t

$$\mathrm{FD}\cdot\frac{1}{\varepsilon_t}\frac{\partial x_{\mathrm{L_t}}(\chi,\tau)}{\partial\chi} + \frac{\partial x_{\mathrm{L_t}}(\chi,\tau)}{\partial\tau} = \frac{1}{Bo}\frac{\partial^2 x_{\mathrm{L_t}}(\chi,\tau)}{\partial\chi^2} \tag{8}$$

$$r\cdot x_{\mathrm{L_t}}(\chi,\tau) = r\cdot x_{\mathrm{L}}(\chi,\tau) + x_{\mathrm{ML}}(\chi,\tau) + 2\cdot x_{\mathrm{ML_2}}(\chi,\tau) \tag{9}$$

which applies for every time unit and every axial position. Mass balances for the other complex forms are not necessary since they are already coupled with the previous Eqs. 2 and 3. FD is a term for flow direction and in a case of adsorption FD is equal to 1, and in a case of desorption is equal to -1. In this way reversibility of the process is obtained. r, α, and Bo are dimensionless parameters found in Eqs. 6–9. r is the concentration ratio of total initial amount of ligand over total initial amount of metal

$$r = \frac{[L_{t,0}]}{[M_{t,0}]}, \tag{10}$$

α gives the ratio of the maximum adsorbent capacity and the initial total metal concentration in the liquid

$$\alpha = \frac{\rho_S\cdot q_S}{[M_{t,0}]} \tag{11}$$

and Bo is the Bodenstein number which gives the ratio convection over axial diffusion:

$$Bo = \frac{u\cdot L}{D_{ax}} \tag{12}$$

Internal Mass Transfer. The internal mass transfer is described with the linear driving force model.[18] The dimensionless form of the internal mass transfer is given as:

$$\frac{\partial\bar{\Gamma}_{\mathrm{M}}(\chi,\tau)}{\partial\tau} = \frac{60N}{Pe_p}(\Gamma_{\mathrm{M}}(\chi,\tau) - \bar{\Gamma}_{\mathrm{M}}(\chi,\tau)) \tag{13}$$

for the M specie, and equivalent equation can be written as well for ML and ML_2. N is the number of particles over the axial direction

$$N = \frac{L}{d_p}, \tag{14}$$

and Pe_P is Peclet number for the particle[18]

$$Pe_p = \frac{u\cdot d_p}{D_{\mathrm{eff}}}. \tag{15}$$

The total loading for all adsorbed species can be written as

$$\bar{\Gamma}_{\mathrm{M_t}}(\chi,\tau) = \bar{\Gamma}_{\mathrm{M}}(\chi,\tau) + \bar{\Gamma}_{\mathrm{ML}}(\chi,\tau) + \bar{\Gamma}_{\mathrm{ML_2}}(\chi,\tau). \tag{16}$$

External Mass Transfer. In our previous work [Djekić T, Tripkovic V, van der Ham AGJ, de Haan AB. Intraparticle diffusion coefficients of $CoCl_2$ in mesoporous functionalized

silica adsorbents. *Adsorption*. (submitted)], we have shown that for a Reynolds number larger than 0.1 the external mass transfer resistance can be neglected.

Initial and Boundary Conditions. In our simulations half of the adsorption column is preloaded to allow broadening of the concentration front during reversible adsorption/desorption cycles. Therefore, the initial conditions used in the model for the first half of column that is preloaded with a catalyst are

$$\begin{aligned}\text{For } \chi = 0 \ldots 0.5^{-} \text{ and } \tau = 0\text{: } & x_{M_t}(\chi,\tau) = 1 \\ & x_{L_t}(\chi,\tau) = 1 \\ & \bar{\Gamma}_M(\chi,\tau) = \Gamma_M(\chi,\tau) \\ & \bar{\Gamma}_{ML}(\chi,\tau) = \Gamma_{ML}(\chi,\tau) \\ & \bar{\Gamma}_{ML_2}(\chi,\tau) = \Gamma_{ML_2}(\chi,\tau).\end{aligned} \tag{17}$$

Since the second half of the bed is set to be empty, the initial conditions for this half of the bed are

$$\begin{aligned}\text{For } \chi = 0.5 \ldots 1 \text{ and } \tau = 0\text{: } & x_{M_t}(\chi,\tau) = 0 \\ & x_{L_t}(\chi,\tau) = 0 \\ & \bar{\Gamma}_M(\chi,\tau) = 0 \\ & \bar{\Gamma}_{ML}(\chi,\tau) = 0 \\ & \bar{\Gamma}_{ML_2}(\chi,\tau) = 0.\end{aligned} \tag{18}$$

By neglecting influence of axial dispersion and due to reversibility of the process boundary conditions of the bed are set as:

$$\text{For FD} = 1 \text{ (adsorption)}\text{: } \quad \chi = 0\text{: } \quad x_{M_t}(\chi,\tau) = 1 \tag{19}$$

$$\chi = 1\text{: } \quad \frac{\partial x_{M_t}(\chi,\tau)}{\partial \chi} = 0 \tag{20}$$

$$\frac{\partial x_{L_t}(\chi,\tau)}{\partial \chi} = 0. \tag{21}$$

$$\text{For FD} = -1 \text{ (desorption)}\text{: } \quad \chi = 0\text{: } \quad x_{M_t}(\chi,\tau) = 0 \tag{22}$$

$$\chi = 1\text{: } \quad \frac{\partial x_{M_t}(\chi,\tau)}{\partial \chi} = 0 \tag{23}$$

$$\frac{\partial x_{L_t}(\chi,\tau)}{\partial \chi} = 0. \tag{24}$$

Model for adsorption of the free ligand

In the second adsorption bed only free ligand is adsorbed. Therefore the stability constant equations are not needed here. Equations used in this model are just listed and no additional explanations are added except that L is the index for the ligand.

Langmuir Adsorption Isotherm for Single Component.

$$\Gamma_L(\chi,\tau) = \frac{\beta_L \cdot x_L(\chi,\tau)}{1 + \beta_L \cdot x_L(\chi,\tau)} \tag{25}$$

Mass Balance for the Liquid Phase in Adsorption Bed.

$$\text{FD} \cdot \frac{1}{\varepsilon_t}\frac{\partial x_L(\chi,\tau)}{\partial \chi} + \frac{\partial x_L(\chi,\tau)}{\partial \tau} + \frac{1-\varepsilon_t}{\varepsilon_t}\alpha\frac{\partial \bar{\Gamma}_L(\chi,\tau)}{\partial \tau} = \frac{1}{Bo}\frac{\partial^2 x_L(\chi,\tau)}{\partial \chi^2} \tag{26}$$

Internal Mass Transfer.

$$\frac{\partial \bar{\Gamma}_L(\chi,\tau)}{\partial \tau} = \frac{60N}{Pe_p}(\Gamma_L(\chi,\tau) - \bar{\Gamma}_L(\chi,\tau)) \tag{27}$$

Initial and Boundary Conditions. Initial and boundary conditions are the same as for the metal adsorption column, except that in this case only the free ligand is adsorbing.

Model implementation

Both models are implemented in the software package gPROMS by Process System Enterprise. The axial domain is discretized using central finite difference method of second order over a uniform grid of 1000 intervals. Numerical method for discretization of time domain is intrinsically embedded in the gPROMS software.

Results and Discussion

Stability of the metal adsorbing column

Data selected to show the stability of the reversible adsorption and desorption are given in Table 2. The half time cycle constant is set as well as the ligand/metal ratio and bed porosities. Catalyst and adsorbent parameters values are in the range that are obtained from our experimental research for $CoCl_2$ adsorption on 2-(2-pyridyl)-ethyl functionalized silica and stability constant measurements [Djekić T, Tripkovic V, van der Ham AGJ, de Haan AB. Intraparticle diffusion coefficients of $CoCl_2$ in mesoporous functionalized silica adsorbents. *Adsorption*. (submitted)].[11,15] Solvent parameters necessary to estimate Reynolds and Bodestein numbers are taken for *N*,*N*-dimethylformamide. 90 m^3 is taken as the reactor volume, and the adsorption bed is selected to be 10% of the reactor volume with the length to diameter ratio of 5. Therefore length of the column L is set to be 6.6 m and column diameter of $D_C = 1.32$ m. N is calculated from Eq. 14 where the particle diameter, d_p, is set to be 10^{-4} m. Peclet number is calculated from Eq. 15 where D_{eff} is taken from our previous research $D_{eff} = 1.95 \times 10^{-10}$ m^2/s, [Djekić T, Tripkovic V, van der Ham AGJ, de Haan AB. Intraparticle diffusion coefficients of $CoCl_2$ in mesoporous functionalized silica adsorbents. *Adsorption*. (submitted)]. and the velocity is recalculated for a given flow of $F = 5 \times 10^{-3}$ m^3/s and column diameter, D_C. The Bodenstein number is calculated as[18]

$$Bo = 0.2\frac{N}{\varepsilon_b}. \tag{28}$$

In our initial simulations it is shown that for Bodenstein numbers larger than 1.74×10^4 axial dispersion can be neglected (Figure 2).

Table 2. Input Base Case Parameters for the Reversible Adsorption/Desorption of the Metal Containing Species[10,14,16]

Parameter	Value	Ref.
Catalyst Parameters		
R	2	–
κ_1	1	(10)
κ_2	1	(10)
Adsorbent Parameters		
β_M	0.8	(14)
β_{ML}	0.4	(14)
β_{ML2}	0.3	(14)
α	925	(14)
Pe_P	1882	(16)
Process Parameters		
$\tau_{1/2}$	5	–
ε_b	0.4	–
ε_t	0.76	–
N	6.6×10^4	–
Re	0.44	–
Bo	1.74×10^4	–

Reversible adsorption/desorption inside one bed is simulated to show stability of the process as well as the constant concentration gradient at the entry ($z/L = 0$) and the exit ($z/L = 1$) of the column. Initially, half of the column ($z/L = 0.05$) is preloaded with catalyst species. Then, the flow through the column is simulated and complex species are adsorbed for a period of $\tau_{1/2}$. Afterwards, the flow direction is reversed and desorption occurs for an equal period, $\tau_{1/2}$. The first cycle is ended. This process is repeated and monitored for 500 cycles.

The total metal concentration profiles in the liquid phase are given after adsorption (Figure 3) for a selection of cycles (1, 100, 200, 300, 400, and 500). The figures show that the concentration profile broadens over time due to unfavorable desorption, and limiting uptake rate during the adsorption. However, the broadening rate of the concentration profile decreases over time which indicates that stable operation can be reached. No decrease of the metal concentration is observed at the entry of the column, as well as no leaching at the end of the column. Both are essential for application of the RFA process.

Influence of catalyst parameters

The first step in designing a RFA process is defining the catalyst properties such as catalyst concentration, stability constants, and initial ligand/metal ratio. The catalyst concentration depends on each application. Therefore the range of catalyst concentrations for which RFA can be applied should be investigated as well as how the concentration influences the concentration profile. Also, depending on the type of metal, ligand, solvent and ligand-metal ratio different distributions of the complex species occurs. Since the complex species (e.g., M, ML, ML_2) have different binding constants it is important to know the catalyst properties to be able to design an affinity adsorbent for the recovery of the catalyst species.

Catalyst properties are specific for each catalytic reaction and cannot be varied to assist a design of the adsorption columns used in the RFA. Therefore, in the following paragraphs we will discuss what kind of effects are observed by altering the above mentioned catalyst properties. These observations will help to design an affinity adsorbents and the corresponding adsorption column.

Metal Inlet Concentration. The concentration of the metal used in homogeneous catalysis depends on its application. For example, typical catalyst's concentrations in hydroformylation processes are between 0.1 and 1.5 mmol/l.[19]

The total metal concentration influences both the distribution of the complex forms, M, ML, and ML_2,[11] and the value of α (Eq. 11). In Figure 4 the total metal concentration profiles are given after 500 cycles for three metal feed concentrations: base case M_t ($M_t = 1$ mmol/l), 2 M_t and 0.5 M_t. The ligand to metal ratio is kept constant (Table 2). Figure 11 shows that at lower concentrations a sharper concentration front is obtained. Therefore, RFA becomes even more applicable for the recovery of low concentration homogeneous catalysts.

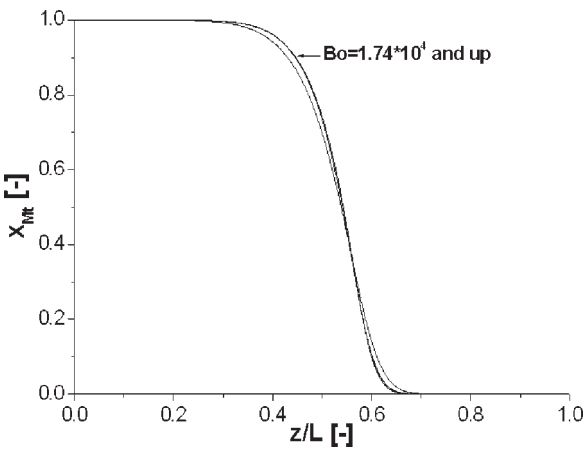

Figure 2. Influence of the axial dispersion on the total metal concentration in the liquid phase after adsorption in the 500th cycles.

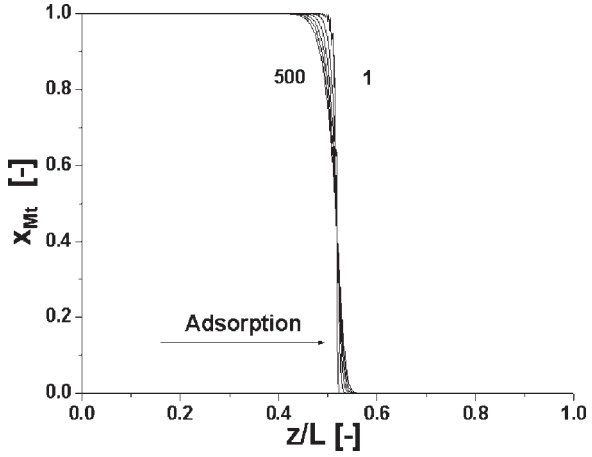

Figure 3. The total metal concentration profile in the liquid phase after the selected number of cycles (1, 100, 200, 300, 400, and 500) for adsorption.

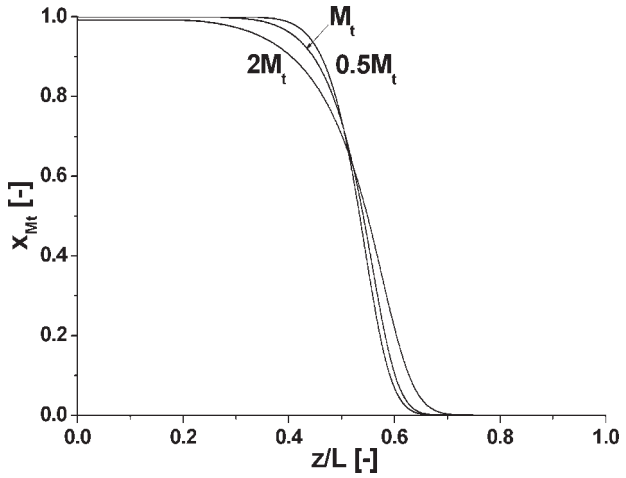

Figure 4. Influence of the metal inlet concentration on the total metal concentration in the liquid phase after adsorption in the 500th cycles.

Stability Constants. Depending on the type of metal, ligand or solvent,[11] different values of stability constants are found to describe the ratio of present complex species. In Figure 5 concentration profiles of the total metal after 500 cycles are given for three values of the stability constants: base case κ_1, κ_2 (Table 2), $10^3\kappa_1$, $10^3\kappa_2$, and $10^6\kappa_1$, $10^6\kappa_2$. In our previous work,[11] we have shown that depending on the type of catalyst the stability constants can vary with 10^6. In Table 3 (columns (a), (c) (d) and (f)), their binding strengths and the relative amounts of M, ML and ML_2 are given for the selected stability constants. Figure 5 shows that an increase of the stability constants results in broadening of the concentration front. This is expected because increasing the stability constant increases the contribution of the ML_2 form, which has the lowest binding strength value.

Therefore the most favorable binding strength that will lead to the sharpest concentration profile should be selected for the form which is dominant (Table 3). This is illustrated in Figure 6. In this case the selected dimensionless stability constant values are $\kappa_{S1} = 10^6$ and $\kappa_{S2} = 10^6$ where the ML_2 specie is dominant (Table 3 column (f)). Two sets of binding constants are compared: binding constants for the base case (Table 3 column (a)) and a new set of binding constants (Table 3 column (b)). In the new set of binding constants we have increased values of binding constants for all forms. The concentration front with an increased β_{ML2} value of 0.8 shows now a significantly sharper profile compared with the concentration profile for the base case. This example also shows that RFA can be applied for a wide range of the stability constants providing that the optimal binding constants are selected.

Ligand to Metal Ratio. Increasing the ligand/metal ratio will shift the equilibrium between the species in the direction of ML_2 [Eq. 1 and Table 3 column (d) and (e)]. Since the ML_2 contribution is increased, a similar effect on the concentration front of the total metal concentration can be noticed as for increasing the stability constant values. Figure 7 shows the total metal concentration profile for two different ligand/metal ratios: r (see Table 2) and $5r$. In both cases the stability constant values were $10^3\kappa_1$ and $10^3\kappa_2$. The concentration profile is broadened by increasing the ligand/metal ratio, which is due to the increase of the amount of ML_2 contributions which adsorbs weaker. This again supports that RFA can be applied for a wide range of catalysts provided that the binding constant is be selected for the dominant specie present.

Influence of adsorbent parameters

The concentration profile of adsorbing species in the adsorption bed mainly depends on the adsorbent properties. The isotherm shape can either bring self-sharpening (favorable isotherm) or self-broadening (unfavorable isotherm) of the concentration front. External and internal mass transfer of the adsorbing species create the "S" shape of the concentration profile, and by reducing these effects sharpening of the concentration profile becomes more pronounced, and at the same time results in a more efficient utilization of the column.[20] Therefore five characteristics are considered for improving the design of the affinity adsorbent

- Binding strength of the adsorbent
- Capacity of the adsorbent
- Mass transfer coefficient
- Particle size of the adsorbent
- Bed porosity.

All five characteristics influence the mass transfer rate inside the particle, while binding strength and adsorbent capacity also influence the shape of the adsorption isotherm. The objective of the following text is to show how altering these four adsorbent characteristics can sharpen the concentration profile inside the bed, and consequently assist in design of a promising affinity adsorbent for the RFA concept.

Binding Constants. The binding constant value influences both the shape of the adsorption isotherm and the mass transfer properties. Increasing the binding strength of the adsorbent slightly increases the mass transfer and sharpens the concentration front in the liquid phase. An

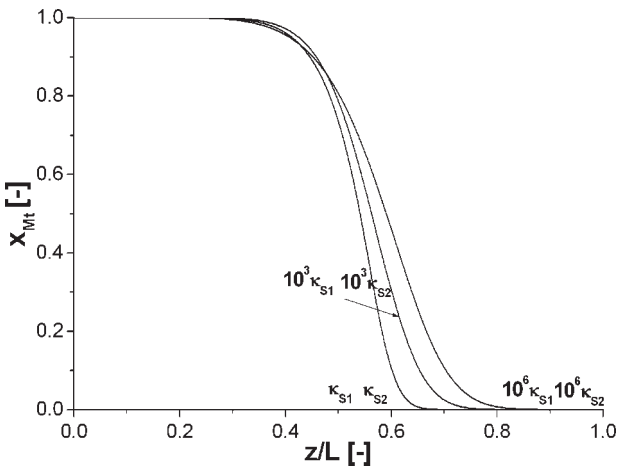

Figure 5. Influence of the stability constants on the total metal concentration in the liquid phase after adsorption in the 500th cycles.

Table 3. Binding Constants [(a) and (b)] and Initial Concentration Distributions [(c)–(f)] of M, ML, and ML_2 Forms for Different Values of Stability Constants and Different Ligand/Metal Ratio

	(a)	(b)	(c)	(d)	(e)	(f)
	β_1 ($r = 2$)	β_2 ($r = 2$)	κ_1, κ_2 ($r = 2$)	$10^3\kappa_1$, $10^3\kappa_2$ ($r = 2$)	$10^3\kappa_1$, $10^3\kappa_2$ ($r = 10$)	$10^6\kappa_1$, $10^6\kappa_2$ ($r = 2$)
x_M	0.8	1.6	0.998	0.33	1.33×10^{-2}	9.4×10^{-4}
x_{ML}	0.4	1.2	2×10^{-2}	0.33	0.108	3.02×10^{-2}
x_{ML2}	0.3	0.8	4×10^{-6}	0.33	0.878	0.968

increase of the binding strength also sharpens the adsorption isotherm profile which can cause sharpening of the wave front during adsorption. On the other hand, desorption becomes more unfavorable: broadening of the concentration profile during desorption and a decrease of the mass transfer rate. Therefore the binding strength should be balanced to find an optimal adsorption/desorption behavior.

These effects are shown in Figure 8 where we studied three binding strengths: the base case, ($\beta_M = 0.8$), increased binding strength ($[4 \cdot \beta_M] = 3.2$) and decreased binding strength ($[0.25 \cdot \beta_M] = 0.2$). It was decided to change only the β_M value since in the base case the free metal specie is dominant (more than 99%) due to low values of stability constants. Compared with base case, β_M, increased binding strength, $4 \cdot \beta_M$, causes sharpening of the profile in the lower concentration range, while broadening in the higher concentration range. For the decreased binding strength, $0.25 \cdot \beta_M$, broadening of the concentration front is noticed for the whole concentration range. These effects can be explained with a combination of continuous adsorption and desorption half-cycles and the presence of a favorable type of adsorption isotherm.

It can be concluded that the binding strength between the adsorbing species and the functionalized groups of the promising affinity adsorbents should be in the range of $\beta_M = 0.8$. This range of β_M values gives the sharpest concentration profile in the adsorption bed where continuous adsorption and desorption are applied.

Adsorbent Capacity. Similar to the binding constant, varying the adsorbent capacity has also two effects: a change of the isotherm's shape and a change of the mass transfer rate. The sharpening speed of concentration profile due to the isotherm profile will decrease by increasing the adsorption capacity. On the other hand, an increase of the adsorption capacity will lead to a faster mass transfer rate and larger bed capacity, and consequently self-sharpening of the concentration front. In case of the linear driving force model, the mass transfer rate increase correlates linearly with the increase in the adsorption capacity. The clear influence of the adsorption capacity on the mass transfer resistance decrease is illustrated in Figure 9. The total metal concentration profiles are shown after 500 cycles for the reference adsorption capacity ($\alpha = 925$), and for cases where the adsorption capacity is doubled ($\alpha = 1850$) and halved ($\alpha = 462.5$). As it can be seen the wave front is sharpening by increasing the value of α. This means that sharpening of the front due to the increase of the mass transfer rate is more pronounced than broadening due to change in isotherm shape. In conclusion, the value of $\alpha = 1850$ gives the sharpest concentration profile. It is a realistic value for the maximum loading that a silica based affinity adsorbent can have.

Effective Diffusion Coefficient. The mass transfer rate inside the adsorbent particle can be enhanced by increasing the value of the effective diffusion coefficient by designing an adsorbent with larger pores (Djekić T, Tripkovic V, van der Ham AGJ, de Haan AB. Intraparticle diffusion coefficients of $CoCl_2$ in mesoporous functionalized silica adsorb-

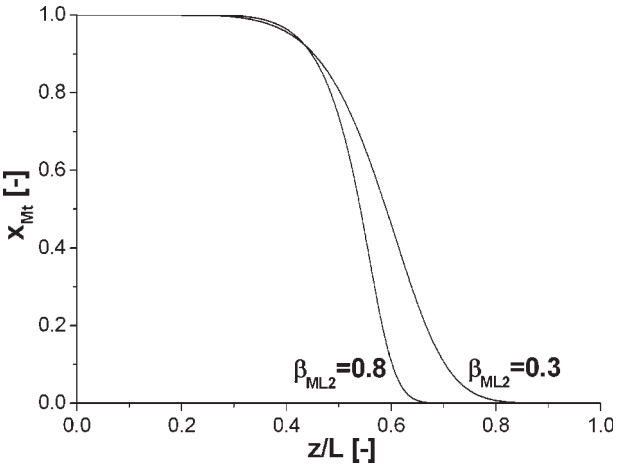

Figure 6. Influence of the binding strengths of M, ML, and ML_2 for $\kappa_{S1} = 10^6$ and $\kappa_{S2} = 10^6$ on the total metal concentration in the liquid phase after adsorption in the 500th cycles.

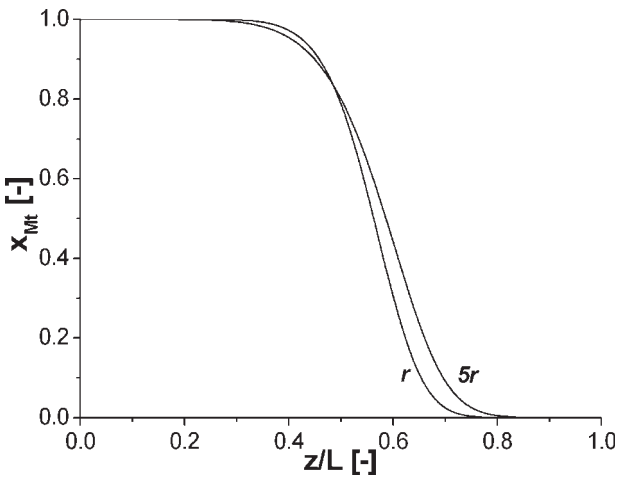

Figure 7. Influence of the ligand/metal ratio on the total metal concentration in the liquid phase after adsorption in the 500th cycles.

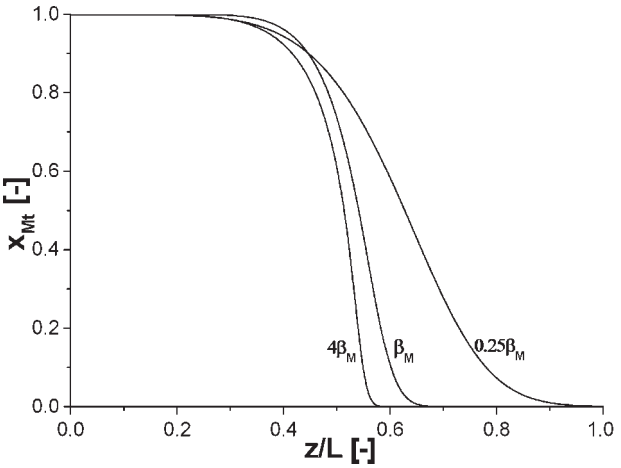

Figure 8. Influence of the bonding strength on the total metal concentration profile in the liquid phase after adsorption in the 500th cycles.

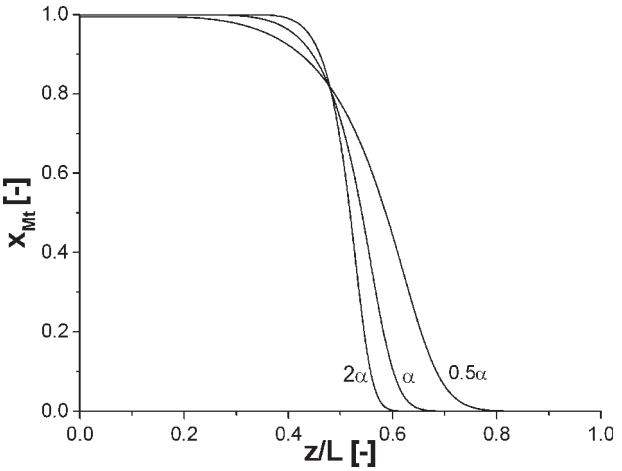

Figure 9. Influence of the adsorbent capacity on the total metal concentration in the liquid phase profile after adsorption in the 500th cycles.

ents. *Adsorption*. (submitted). The effective diffusivity in our dimensionless model is described by the Peclet number for particles, Pe_P (Eq. 15). Figure 10 shows the total metal concentration profiles for three different Pe_P numbers: Pe_P = 1882, $5 \cdot Pe_P = 9410$, and $0.2 \cdot Pe_P = 376.4$. As expected a decrease of Pe_P numbers (larger effective diffusion coefficients or a smaller particle diameter) enhances mass transfer. Since dependence of the concentration change on Pe_P number is exponential (Eq. 13), it can explain the nonlinear change of the concentration profile. Therefore it can be expected that at small Pe_P numbers concentration profile will not change its shape any further.

The sharpest concentration profile is reached for the Peclet particle number $Pe_P = 376.4$. This value is also a realistic value that can be reached by designing a silica based affinity adsorbent with large and uniform pores of e.g. 90 Å in diameter.

Particle Size. Mass transfer between the liquid and solid phase can be enhanced by decreasing the particle size of the adsorbent (see Eqs. 13–16 and Figure 12). Change of the particle size influences dimensionless numbers, Pe_P and N. Influence of Pe_P change is discussed in previous part (Effective diffusion coefficient) where it was shown that for smaller Pe_P numbers sharper profile can be reached. Figure 11 shows that increasing the N value (increasing column length or decreasing particle size) a sharper concentration profile is reached. Figure 12 illustrates the sharpening of the concentration front by decreasing the particle size, where effects of changing two dimensionless numbers, Pe_P and N, are combined. As a result it is concluded that the smallest particle diameter should be selected for the best design of an affinity adsorbent.

The practical problem that arises by decreasing the particle size is an increase of the pressure drop across the column. In this work, the pressure drop is estimated by the Ergun equation for a fixed bed:

$$\frac{\Delta P}{L} = \frac{150\mu(1-\varepsilon_b)^2 u}{\varepsilon_b^3 \cdot d_p^2} + \frac{1.75(1-\varepsilon_b)\rho \cdot u^2}{\varepsilon_b^3 \cdot d_p} \qquad (29)$$

Table 4 shows the calculated pressure drop for the base case ($d_p = 100$ μm) and two cases with different particle sizes ($d_p = 50$ μm and $d_p = 200$ μm). Particle size tremendously influences pressure drop. The allowed pressure drop usually depends on each specific application. For processes that work under high pressures (higher than 20 bars) it is recommended to use particle size of $d_p = 200$ μm ($N = 3.3 \times 10^4$ and $Pe_P = 3764$) as a realistic particle size. For other applications even larger particle sizes are needed or other bed optimizations, such as a reduction of bed length or an increase of bed porosity.

Bed Porosity. Porosity of the bed depends on the particle size and shape. Influence of the concentration profile on bed porosities is studied for 3 values: 0.3, 0.4, and 0.5, where particle size is kept constant ($d_p = 100$ μm). It is expected that by decreasing the bed porosity the concentration profile is sharpening since the contribution of the solid phase

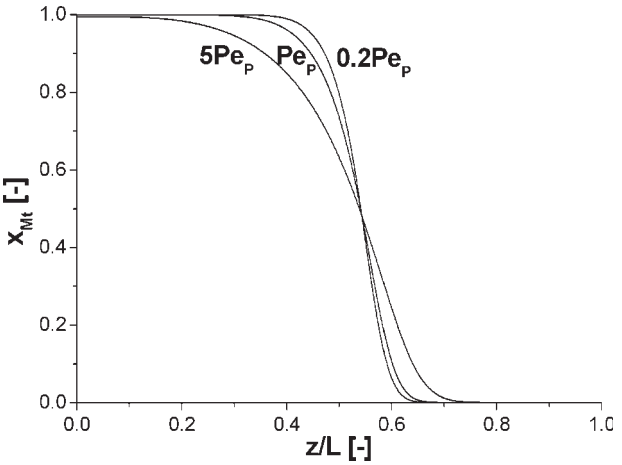

Figure 10. Influence of the effective diffusion coefficient on the total metal concentration in the liquid phase after adsorption in the 500th cycles.

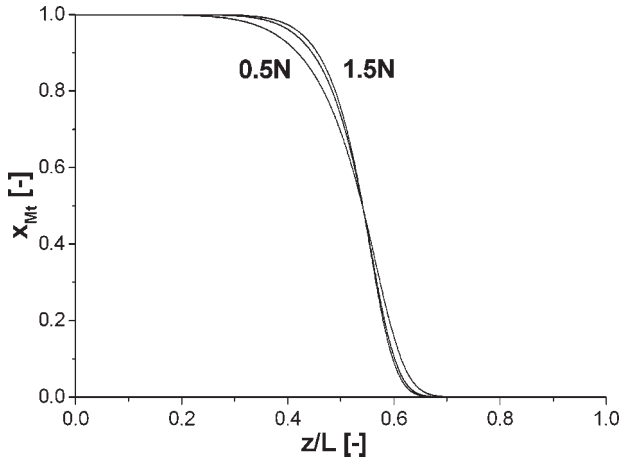

Figure 11. Influence of the N value on the total metal concentration in the liquid phase after adsorption in the 500th cycles.

increases (Figure 13). On the other hand, pressure drop inside the bed increases by decreasing the bed porosity (Eq. 25). For tested porosities ($\varepsilon_b = 0.3$, $\varepsilon_b = 0.4$, and $\varepsilon_b = 0.5$) calculated pressure drop is respectively 53, 16.5, and 5.8 bar. To avoid large pressure drops influences of bed porosity and particle size have to be combined: smaller bed porosity asks for larger particle size and vice versa.

Therefore, we recommend to select particle size of $d_p = 200$ μm and porosity of $\varepsilon_b = 0.5$ to decrease pressure drop to around 1.5 bars.

Silica Adsorbent Design. Conclusions for silica based adsorbent design are given in Table 5. General conclusions and possible material or system limitations are given for the main five adsorbent characteristics. Table 5 should be a guideline for the design of adsorbents which will be applied in the RFA process. In the second column general conclusions drawn from the previous simulations are given, while in the third column material and system limitations are pointed. Designing an adsorbent for the RFA process, one should follow general conclusions, but in the same time comprise both material and process limitations.

Table 4. Influence of the Particle Size on the Pressure Drop Across the Column

d_p (μm)	100	50	200
N	6.6×10^4	1.32×10^5	3.3×10^4
Pe_P	1882	941	3764
ΔP (bar)	16.5	65	4.1

Design of the ligand column

In the first column, the metal adsorbing bed, a part of the ligand is always adsorbed through adsorbing ML and ML_2 species. In the second column only the free ligand is adsorbed. Therefore in this bed competitive adsorption of different forms, present in the first bed, is excluded. However, depending on each application the ligand can be in a large excess (ligand/metal ratio r can be as high as 100[17]). Objective of the following work is to show stability of the ligand adsorbing column and to study up to which excess of ligand the RFA process can be applied.

Stability of the Process. Parameters used in simulating the reversible adsorption and desorption of the free ligand are given in Table 6. These values are based on the conclusions drawn in the previous part of our study of adsorbent parameters. Figure 14 confirms that a stable operation is obtained also for the reversible adsorption and desorption of the free ligand. As well as in the metal column the broadening speed of the concentration profile due to unfavorable desorption, and limiting uptake rate decreases over time which finally results in a stable operation. Additionally, there was no decrease in the ligand concentration front at the entry of the column, as well as no leaching at its exit.

Ligand Concentration. In many homogeneous catalytic reactions the ligand is used in excess,[19] and therefore the ligand concentration can vary depending on each specific application. In this simulation the maximal ligand concentration that can be recovered in an adsorption column based on

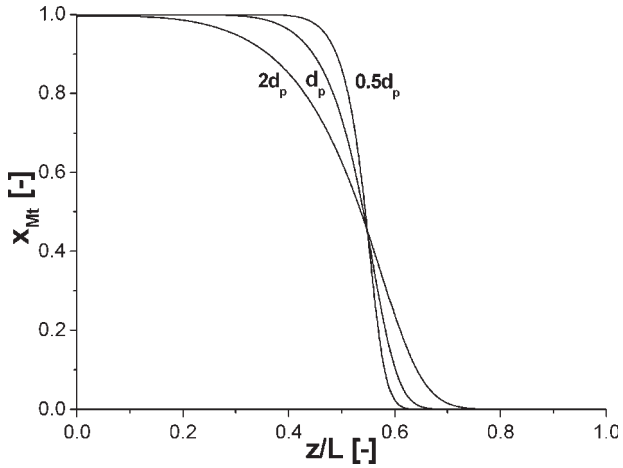

Figure 12. Influence of the particle diameter on the total metal concentration in the liquid phase after adsorption in the 500th cycles.

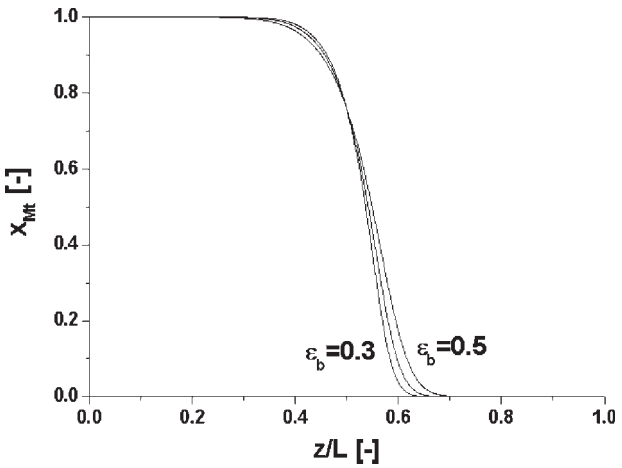

Figure 13. Influence of the bed porosity on the total metal concentration in the liquid phase after adsorption in the 500th cycles.

Table 5. Overview of the Adsorbent Design

	General Conclusions	Material/System Limitation
Binding constants (b)	≈ 0.8 m^3/mol ($\beta = 0.8$)	No
Adsorbent capacity (q_s)	Maximal	$\approx 10^{-3}$ mol/g ($\alpha = 1850$)
Effective diffusion coefficient (D_{eff})	Maximal	$\approx 6 \times 10^{-10}$ m^2/s ($Pe_P = 376.4$) $D_{eff} = \frac{1}{\text{surfacearea}}$
Particle size (d_p)	Minimal	Allowable pressure drop
Bed porosity (ε_b)	Minimal	Allowable pressure drop

parameters given in Table 6 is studied. Figure 15 shows ligand concentration profiles after 500 cycles for different initial concentrations ($2L_t$, L_t, $0.5L_t$, and $0.25L_t$). For all initial concentrations no leaching of the ligand was detected. However for $2L_t$ a decrease in the ligand concentration at the entry of the column was found. At the low ligand concentrations profile is very sharp, while in the higher region profile is broadening. Therefore, we preloaded 70% of column and with this condition ligand with $2L_t$ concentration could be kept inside the column, while already at $3L_t$ decrease in the ligand concentration at the entry of the column were as well found (Figure 16). In conclusion, ligand concentrations of $L_t = 4$ mmol/l or lower can be recovered by RFA using adsorbent properties given in this simulation. Otherwise, if the ligand concentration is higher than $3L_t$ either the column parameters should be changed (e.g. increasing the preloading part or column size) or other technique for the recovery of the free ligand might be needed.

Example: hydroformylation process

The BASF hydroformylation process was selected as a demo-process to design an adsorption column for the recovery of the metal species. In this process rhodium is used as a metal centre while PPh_3 as a ligand. Reactor volume ($V_{reactor}$), flow rate (F), and concentration of rhodium (C_{Rh}) are taken from Cornils and Hermann[17] (Table 7). Adsorbent parameters are taken from the conclusions drawn in the previous part of the article. Since stability constants of this catalyst are unknown it is chosen to simulate process where the catalyst complex is present in only one form, ML_3.

Table 8 shows different combinations of maximal operation times for different volumes of adsorption bed as well as for different designs (L/D_c ratio). Three bed volumes are studied: 10% (column (a)), 3% (column (b)) and 1% (column (f)) of the reactor volume. By increasing the bed volume a longer maximum operation time is obtained. For the bed volume of 1.35 m^3 after $\sim$51 days, a breakthrough at the entry of the bed occurs. This time is changed to 1190 days by increasing the bed volume 10 times. On the other hand, increasing the bed volume will result in larger investments both in the equipment and preloading of the adsorbent by catalyst.

One way to extend the maximal operation time is by keeping the same bed volume and changing the bed design. This is shown in Table 8 (columns (b) and (c)) where the maximum operation times are given for constant bed volumes (4.05 m^3) but in the first case the ratio of bed length over bed diameter is 5 and in the second 10. The maximal operating time is extended from 254 to 355 days. This has its penalty by increasing the pressure drop in the system from 0.85 to 2.2 bar.

The operation time would also got increased if the process would be changed by introducing a new, more effective catalyst which has higher TON (less of catalyst concentration is needed). For the bed volume equal to 3% of the reactor volume and an initial catalyst concentration of 0.8 mmol/l (column (b)) the estimated maximal half cycle time, $\tau_{1/2,\ max}$, is 25 and maximal operation time is 254 days. If the initial metal concentration decreases with 50% (column (d)), the half cycle time increases to 35 and the maximum operating time is now 356 days. At the end, an increase in L/D_c and a decrease in catalyst concentration are applied. The results show that the maximum operating time is extended to $\sim$507 days (column (e)).

It can be concluded that an adsorption column with a volume of the 3% of reactor volume is sufficient for fully recovery of the metal containing species in the BASF hydroformulation process. Therefore the total bed volume for two adsorption beds applied in the RFA should be 6%. The maxi-

Table 6. Input Base Case Parameters for the Reversible Adsorption/Desorption of the Free Ligand

Parameter	Value
Adsorbent Parameters	
β_L	1.6
α	1850
Pe_P	376.4
Process Parameters	
$\tau_{1/2}$	5
ε_b	0.4
N	6.6×10^4
Bo	1.74×10^4

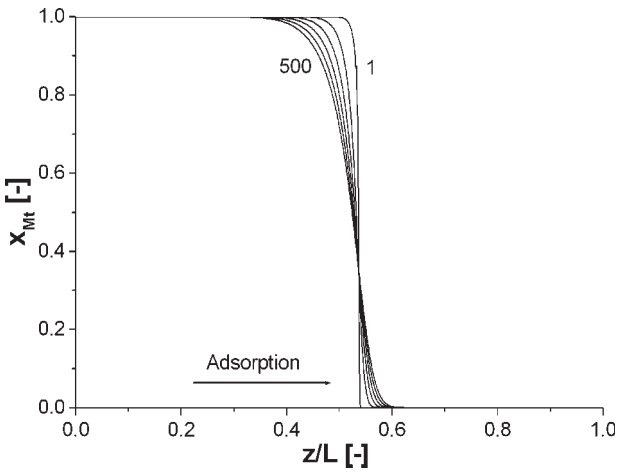

Figure 14. The ligand concentration profile in the liquid phase for the selected number of cycles (1, 100, 200, 300, 400, and 500) after adsorption.

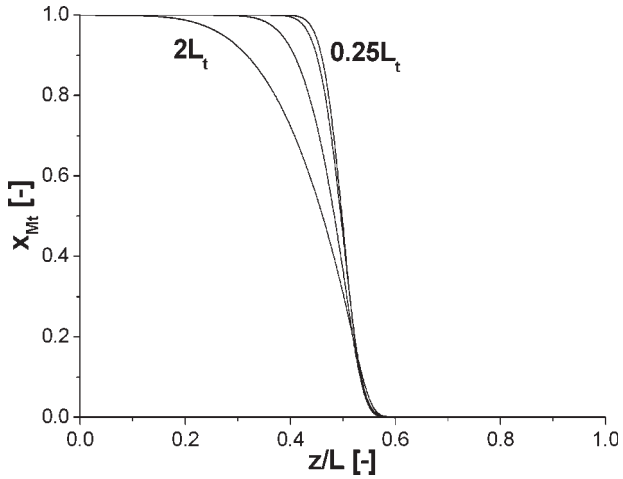

Figure 15. Influence of the ligand inlet concentration on ligand concentration in the liquid phase after adsorption in the 500th cycles.

mum operating time can be increased by increasing the L/D_c ratio and by introducing more efficient catalysts.

Conclusions

Silica adsorbent design and modeling of the reversible adsorption/desoprtion process for the recovery of homogeneous catalysts are studied in this work. The following major conclusions are drawn:

- Stable operation for 500 cycles can be reached for the reversible adsorption/desorption process where no leaching of the catalyst species is noticed;
- Silica based adsorbent which will provide a sharpening of the concentration profile inside the bed should have binding constant of around 0.8 m^3/mol ($\beta = 0.8$), adsorbent capacity of 10^{-3} mol/g ($\alpha = 1850$), effective diffusion coefficient in range of 6×10^{-10} m^2/s ($Pe_P = 376.4$), and minimal particle size and bed porosity with limitation of tolerable pressure drop.
- For Bodenstein numbers larger than $1.74 \cdot \times 10^4$ axial dispersion can be neglected inside the bed;
- The RFA process can be applied for wide ranges of the stability constants and becomes even more applicable for the recovery of homogeneous catalysts that have a lower metal concentration;
- Simulation of the recovery of Rh catalyst in the BASF hydroformylation process required total adsorption bed volume of 6% of reactor volume.

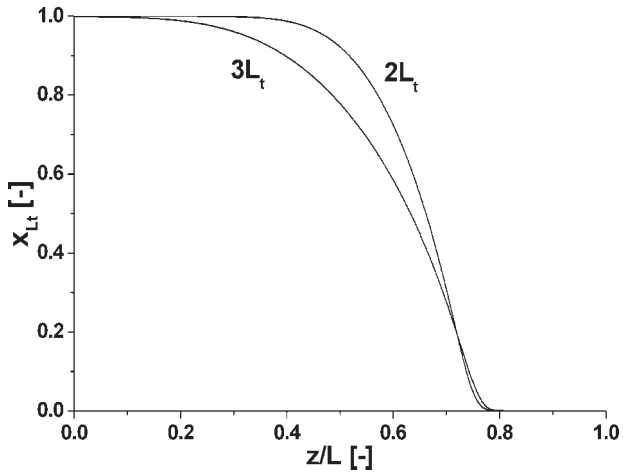

Figure 16. Influence of the ligand inlet concentration on ligand concentration in the liquid phase after adsorption in the 500th cycles with a 70% preloaded column.

Table 7. BASF Hydroformylation Data[18] and Parameters Selected

$V_{reactor}$ (m^3)	135
F (m^3/s)	2.3×10^{-3}
C_{Rh} (mol/m^3)	0.8
β_M	0.8
A	1850
ε_b	0.4

Table 8. Maximal Operation Time for Metal Adsorbing Column

	(a)	(b)	(c)	(d)	(e)	(f)
$V_{reactor}$ (m^3)	135	135	135	135	135	135
V_{bed} (%$V_{reactor}$)	**10**	**3**	3	3	3	**1**
$C_{catalyst}$ (mmol/l)	0.8	0.8	0.8	**0.4**	**0.4**	0.8
L/D_c	5	5	**10**	5	**10**	5
N^o *cycles*	500	500	500	500	500	500
$\tau_{1/2,\ max}$	35	25	35	35	50	15
$t_{total,max}$ (days)	**1190**	**254**	**355**	**356**	**507**	**50.8**
ΔP (bar)	0.54	0.85	2.2	0.85	2.2	1.27

Acknowledgments

This project is financially supported by Dutch Organisation for Scientific Research-Foundation of technology and science (NWO-STW). Acknowledgments to the following companies for the contributions in this project: Sasol, Engelhard, Akzo Nobel, Degussa and TNO. We want to acknowledge fruitful discussions during preparation of this paper with Louis van der Ham and Hans Bosch from University of Twente and Frank Peters from Eindhoven University of Technology.

Notation

b_L = adsorption binding strength for component L [m^3/mol]
b_M = adsorption binding strength for component M [m^3/mol]
b_{ML} = adsorption binding strength for component ML [m^3/mol]
b_{ML2} = adsorption binding strength for component ML_2 [m^3 /mol]
Bo = bodenstein number ($= u \cdot d_p/D_{ax}$) [-]
$C_{catalyst}$ = concentration of the catalyst [mol/m^3]
C_{Rh} = rhodium concentration [mol/m^3]
D_{ax} = axial dispersion coefficient [m^2/s]
D_c = column diameter [m]
D_{eff} = effective diffusion coefficient [m^2/s]
d_P = particle diameter [m]
F = flow [m^3/s]
FD = flow direction [-]
i = index for L, M, ML and ML_2 [-]
K_{s1} = stability constant for the first complexation step [m^3/mol]
K_{s2} = stability constant for the second complexation step [m^3/mol]
L = length of the column [m]
$[L_{t,0}]$ = initial total concentration of the free ligand [mol/m^3]
[M] = concentration of the free metal [mol/m^3]
[ML] = concentration of the ML complex [mol/m^3]

$[ML_2]$ = concentration of the ML_2 complex [mol/m^3]
$[M_t]$ = total concentration of all metal containing forms [mol/m^3]
$[M_{t,0}]$ = initial total concentration of all metal containing forms [mol/m^3]
N = number of particle over the axial distance $(= L/d_p)$ [-]
ΔP = pressure drop [bar]
Pe_P = Peclet number for particle $(= [u \cdot d_p]/D_{eff})$ [-]
q_i = loading of free ligand, free metal, ML and ML_2 on the adsorbent at the interface [mol/kg]
$\overline{q}_i$ = averaged loading of free ligand, free metal, ML and ML_2 on the adsorbent [mol/kg]
q_S = maximum loading on the adsorbent [mol/kg]
r = ratio between total ligand and total metal concentration $(= [L_{t,0}]/[M_{t,0}])$ [-]
$t_{1/2}$ = half cycle time [s]
$t_{total,max}$ = maximal total operation time [days]
u = superficial velocity $(= [F \cdot 4]/[D_C^2 \cdot \pi])$ [m/s]
x_L = dimensionless concentration of the free ligand $(= [L]/[L_{t,0}] = [L]/[M_{t,0}] \cdot r)$ [-]
x_M = dimensionless concentration of the free metal $(= [M]/[M_{t,0}])$ [-]
x_{ML} = dimensionless concentration of the ML complex $(= [ML]/[M_{t,0}])$ [-]
x_{ML2} = dimensionless concentration of the ML_2 complex $(= [ML_2]/[M_{t,0}])$ [-]
x_t = dimensionless concentration of the total concentration of all metal containing forms $(= [M_t]/[M_{t,0}])$ [-]
V_{bed} = bed volume [m^3]
$V_{reactor}$ = reactor volume [m^3]
z = axial distance [m]
β_L = dimensionless adsorption binding constant for L $(= b_L \cdot [L_{t,0}])$ [-]
β_M = dimensionless adsorption binding constant for M $(= b_M \cdot [M_{t,0}])$ [-]
β_{ML} = dimensionless adsorption binding constant for ML $(= b_{ML} \cdot [M_{t,0}])$ [-]
β_{ML2} = dimensionless adsorption binding constant for ML_2 $(= b_{ML_2} \cdot [M_{t,0}])$ [-]
Γ_i = dimensionless loading of free ligand, free metal, ML and ML_2 on the adsorbent at the particle interface $(= q_i/q_S)$ [-]
$\overline{\Gamma}_i$ = dimensionless averaged loading of free ligand, free metal, ML and ML_2 on the adsorbent $(= \overline{q}_i/q_S)$ [-]
ε_b = porosity of the bed [-]
ε_t = total porosity [-]
κ_1 = dimensionless stability constant, K_{s1}, $(= K_{S1} \cdot r \cdot [M_{t,0}])$ [-]
κ_2 = dimensionless stability constant, K_{s2}, $(= K_{S2} \cdot r \cdot [L_{t,0}])$ [-]
μ = viscosity [Pa s]
ρ_S = density of the adsorbent [kg/m^3]
$\tau_{1/2}$ = dimensionless time $(= [t \cdot u_{sup}]/L)$ [-]
$\tau_{1/2,max}$ = dimensionless maximal half cycle time [-]
χ = dimensionless axial distance $(= z/L)$ [-]

Literature Cited

1. Boreskov GK, Matros YuSh. Flow reversal of reaction mixture in a fixed catalyst bed-a way to increase the efficiency of chemical processes. *Appl Catal*. 1983;5:337–343.
2. Matros YuSh, Noskov AS, Chumachenko VA, Goldman OV. Theory and application of unsteady catalytic detoxication of effluent gases from sulphur dioxide, nitrogen oxides and organic compounds. *Chem Eng Sci*. 1988;43:2061–2066.
3. Chan FL, Keith JM. Designing reverse-flow packed bed reactors for stable treatment of volatile organic compounds. *J Environ Manage*. 2006;78:223–231.
4. Smit J, Bekink GJ, van Sint Annaland M, Kuipers JAM. Experimental demonstration of the reversible flow catalytic membrane reactor concept for energy efficient syngas production, Part 1: influence of operationg conditions. *Chem Eng Sci*. 2007;62:1239–1250.
5. Gosiewski K. Dynamic modelling of industrial SO_2 oxidation reactors, Part II: *model of a reverse Flow reactor*. *Chem Eng Process*. 1993;32:233–244.
6. Dubber MJ, Kanfer I. Application of reverse-flow micellar electrokinetic chromatography for the simultaneous determination of flavonols and terpene trilactones in Ginko biloba dosage forms. *J Chromatogr A*. 2006;1122:266–274.
7. Gilron J, Waisman M, Daltrophe N, Pomerantz N, Milman M, Ladizhansky I, Korin E. Prevention of precipitation fouling in NF/RO by reverse flow operation. *Desalination*. 2006;199:29–30.
8. Govender S, Jacobs EP, Leukes WD, Odhav B, Pillay VL. Towards an optimum spore immobilisation strategy using *Phanerochaete chrysosporium*, reverse filtration and ultrafiltration membranes. *J Membr sci*. 2004;238:83–92.
9. Dunnewijk J, Bosch H, de Haan AB. Reverse flow adsorption: integrating the recovery and recycling of homogeneous catalysts. *Sep Purif Technol*. 2004;40:317–320.
10. Scarpello JT, Nair D, dos Santos LMF, White LS, Livingston AG. The separation of homogeneous organometallic catalysts using solvent resistant nanofiltration. *J Membr Sci*. 2002;5180:1–15.
11. Djekić T, Zivkovic Z, van der Ham AGJ, de Haan AB. Determination of the stability constants for cobalt, nickel and palladium homogeneous catalyst complexes containing triphenylphosphine ligands. *Appl Catal A*. 2006;312:144–152.
12. Dunnewijk J. Reverse Flow Adsorption Technology for Homogeneous Catalyst Recycling. PhD thesis. University of Twente, The Netherlands, 2006.
13. Dunnewijk J, Bosch H, de Haan AB. Adsorption kinetics of CoCl2 and PPh3 over macroreticular and gel type adsorbents by a generalized ZLC method. *Chem Eng Sci*. 2006;61:4813–4826.
14. Dunnewijk J, Bosch H, de Haan AB. Integrated recovery and recycling of homogeneous catalysts by reverse flow adsorption: selection of suitable adsorbents. *Adsorption*. 2005;11:521–526.
15. Djekić T, van der Ham AGJ, Bosch H, de Haan AB. Adsorption of homogeneous catalysts over functionalized silica adsorbents: modelling of the competitive adsorption isotherms. *Chem Eng Sci*. 2007;62:2032–2039.
16. Djekić T, van der Ham AGJ, de Haan AB. Evaluation of functionalized silica's for the adsorptive recovery of homogeneous catalysts through intereaction with the metal centre. *J Chromatogr A*. 2007; 11420:32–38.
17. Cornils B, Hermann WA, editors. *Applied Homogeneous Catalysis with Organometallic Compounds: a Comprehensive Handbook*. Weinheim: Wiley-VCH, 2002:82–83.
18. Guiochon G, Felinger A, Shirazi SG, Katti AM. *Fundamentals of Preparative and Nonlinear Chromatography, 2nd ed*. Amsterdam: Academic Press, 2006:151–219.
19. van Leeuwen PWNM. *Homogeneous Catalysis- Understanding the Art*. Dordrecht: Kluwer Academic Publishers, 2004:7–8.
20. Bosch H, de Haan AB. *Fundamentals of Industrial Separations, 2nd ed*. Enschede, Netherlands: University Twente, 2007:6-1–6-23. ISBN 978-90-810973-2-1.

Manuscript received Sept. 13, 2007, revision received Mar. 20, 2008, and final revision received May 2, 2008.